Morphology and Raman spectra of aerodynamically classified soot samples

Alberto Baldelli, Steven Nicholas Rogak[1]

[1]Department of Mechanical Engineering, University of British Columbia
6250 Applied Science Ln #2054, Vancouver, BC V6T 1Z4

Correspondence to: Alberto Baldelli (baldelli.alberto@yahoo.com)

Supplementary material

Here we describe some practical issues related to the aerosol sampling, TEM analysis, and choice of aerosol generation system. Several variants of aerosol generation were tested, resulting in slightly different Raman spectra, as discussed below.

Aerosol sampling on ELPI+ stages

Figure S.1 shows the images of soot aerosols deposition on each stage of ELPI+ impactor. The collection time was set at 10 minutes to produce a visible deposit, needed for Raman microscopy. Soot production conditions are set as follows: dilution flow rate of 4 lpm, and ethylene flow rate of 0.13 lpm.
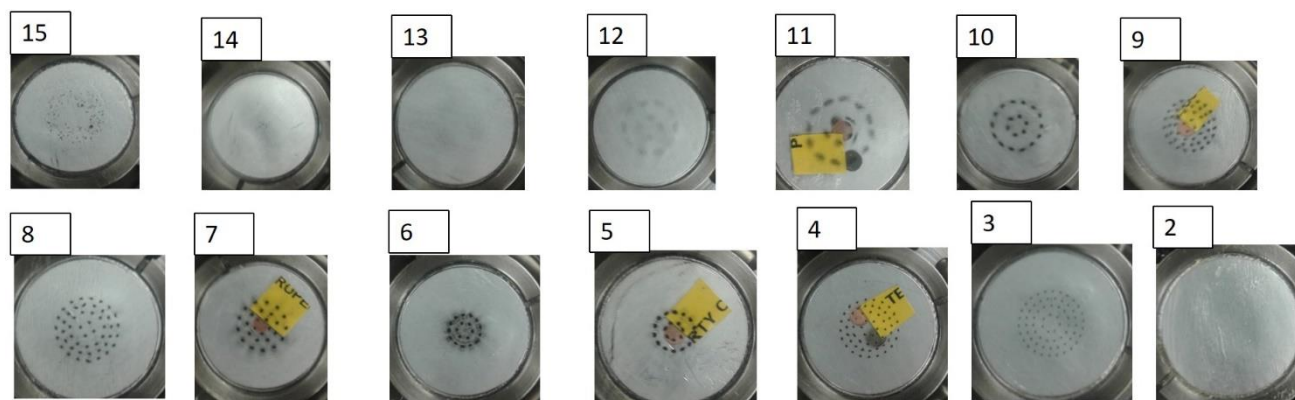
Figure S.1 Images of each stage of ELPI+ impactor using the system introduced in Figure 1 in the main publication.

Alternative configurations and operating conditions of inverted burner

The results described in the main manuscript used bottled commercial air for the burner combustion air. However, before this some variants were used with filtered compressed building air supplied to the burner. In configuration b ("Building Air without Thermodenuder"), we were concerned that the organic content based on TC/EC was too large, so tests were conducted with

5   configuration c ("Building Air with Thermodenuder").

a) Bottled air

The experimental setup using the bottled air is introduced in Figure 1 of the main publication, and is the basis of the Raman spectra in the main publication. Additional details are shown below. Table S.1 shows the centers of the fitted peaks for each band of the Raman spectra shown in the main publication (Figure 7). The repeatability of the peak centers shows the stability

10   of the Raman spectra deconvolution.

Table S.1 Centers of the fitted peaks for each band of the Raman spectra for test cases shown in Figure 6 and 7 in the main publication.

Stages	D1	D3	D2	D4	G
3	1315.5	1519.3	1613.6	1159.3	1583.8
4	1314.2	1521.0	1611.5	1157.1	1583.4
5	1310.5	1519.1	1609.5	1150.3	1579.9
6	1311.1	1516.6	1608.9	1156.6	1579.3
7	1313.0	1521.2	1610.9	1155.3	1581.4
8	1313.9	1521.8	1610.5	1155.4	1581.1
9	1312.0	1503.4	1619.5	1169.8	1587.1
10	1314.5	1502.2	1619.5	1169.8	1588.8
11	1319.0	1507.3	1619.5	1176.3	1589.7
Total	1315.1	1510.9	1620.8	1169.8	1588.0

A constant flame is achieved after about 30 minutes from the flame ignition. Raman spectra of soot produced at the ignition shows a possible presence of organics (Figure S.2). A peak at about 2050 cm^{-1} is identified. Previous literature references

15   define that this peak could correspond to oxidized polyaromatic hydrocarbons (PAHs) (Cloutis et al., 2016; Cordeiro and Corio, 2009). Oxidized PAHs are obtained by a chemical reaction of PAHs, precursors of soot, and NOx, SOx, or oxygen (Nowakowski et al.). The correlation of this peak with oxidized PAHs is speculative.
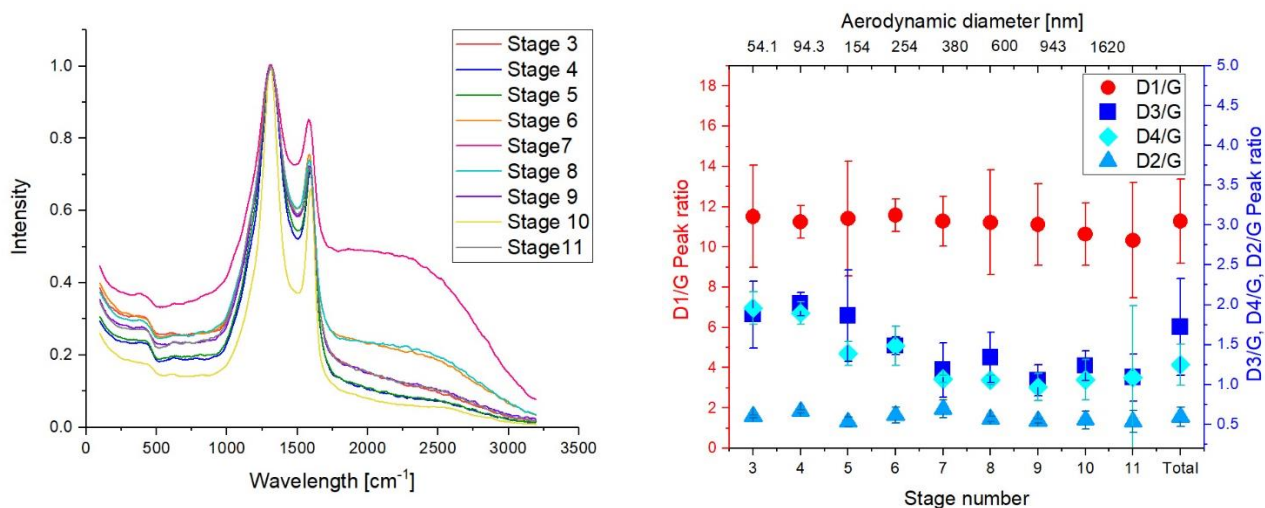
Figure S.2 Raman spectra and peak ratios of soot collected ethylene flow rate of 0.13 lpm and use of a bottled air at 10 lpm. Samples were collected at directly after ignition using the setup system shown in Figure 1 in the main publication.

Even with the likely presence of organics for the non-stabilized flame, the D3/G and D4/G peak ratios show a decrease with the stage number (as for the stabilized samples of the main publication).

Another potential artifact considered in this work was the effect of the substrate on the Raman spectra. All Raman spectra have been deconvoluted using Origin Pro, using several baseline subtraction approaches. The baseline correction in the main publication subtracts the best-fit scaling of the clean titanium substrate signal. This shows a slight peak that overlap with peaks D1 and D3 in the soot Raman spectrum. The alternative considered (used initially) was a simple linear baseline subtraction. Figure S.3 shows the Raman peak ratios for this simplified approach. By comparing Figure S.3 with Figure 7 in the main publication, the lower stages show lower D/G peak ratios, while higher stages show a slightly higher D/G peak ratio. The middle stage (from 6 to 8) shows the highest soot aerosols mass content and, thus, are less affected by the Raman signal of titanium substrates. In other words, the simplified baseline correction yields the same qualitative trends, but they are not as clear as when the actual titanium spectrum is used in the correction.

3
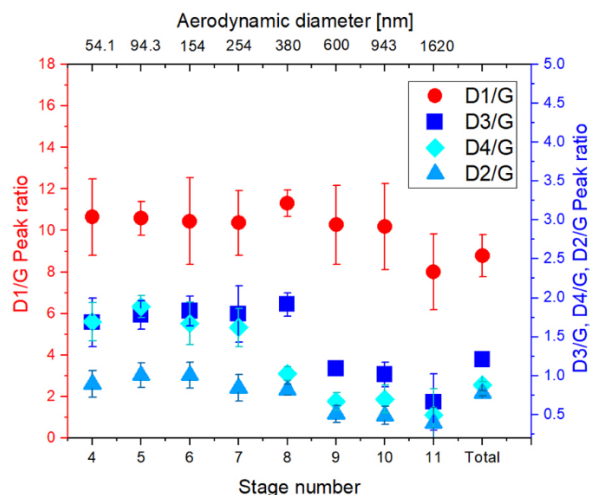
Figure S.3 Raman peak ratios of soot aerosols produced by the inverted burner fed with 0.13 lpm of ethylene and 10 lpm of bottle air and with the operating system shown in Figure 1 in the main publication. The Raman spectra have been deconvoluted *without* using the titanium substrate Raman signal as baseline.

b) Building air without thermodenuder

In these experiments, building compressed air was used for the flame air supply (Figure S.4). Flow rates of ethylene, air, and collection system were unchanged. This air is cleaned using a system of three particulate filters and a silica bead dehumidifier.
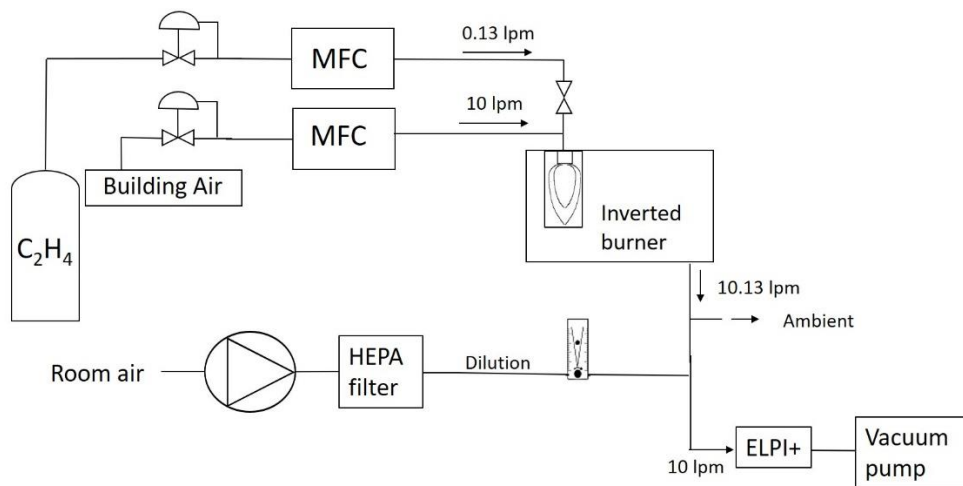
Figure S.4 Schematic of the experimental setup involving the use of the building air as source of the inverted burner combustion flame.

5

Using this experimental setup, the morphology of segregated soot aerosols was analyzed. Two air flow rates have been considered: 0.09 and 0.13 lpm. A minor difference is encountered between the two different production flow rates; the case of 0.09 lpm shows slightly lower peak ratios and a stronger difference between lower and upper stages of the impactor. Reasons can be found in the possible difference in the organics present in the flame. A higher content of elemental carbon could show

5   a lower amount of amorphous carbon contained in the sample. Thermal-Optical-Transmittance (TOT) is a common technique to analyze organic carbon (OC), elemental carbon (EC), carbonate carbon (CC), total carbon (TC) (Lappi and Ristimäki, 2017). TOT has been conducted on the total exhaust of the inverted burner collected on glass fiber filters. Results shows an average ratio of elemental and organic carbon (EC/OC) of 0.91 and 0.87 when the flow rate production is 0.13 lpm and 0.09 lpm respectively (Kazemimanesh et al., 2018).

10   Figure S.5 shows the distribution of primary particles respect to the projected equivalent diameter for soot collected using building air as feeding gas. Similar data are shown in Figure 6 in the main publication; results obtained by analyzing soot aerosols generated with an ethylene flow rate of 0.09 lpm are shown.
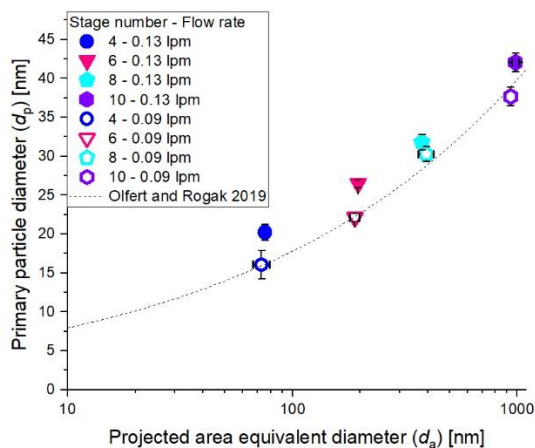
Figure S.5 Distribution of primary particles respect to the projected area equivalent diameter for stages 4, 6, 8 and 10. Building air was set at 10 lpm. Two ethylene flow rates, 0.09 and 0.13 lpm have been considered and have been shown as full and empty symbols respectively.

Figure S.6 shows the Raman peak ratio of soot nanoparticles generated by an inverted burner fed with 0.13 lpm a) and 0.09 lpm b) of ethylene gas using the system shown in Figure S.4. The trend of Raman peak ratios (D1/G, D2/G, D3/G, and D4/G) is opposite compared to the ones shown in Figure 8 in the main publication. We estimate that the reason of this trend is due to the presence of hydrocarbons in building air. These hydrocarbons could increase the disordered content in the soot aerosols at certain aerodynamic diameters. The reasons of the trend encountered in Figure S.6 are unclear and more investigations might be needed.
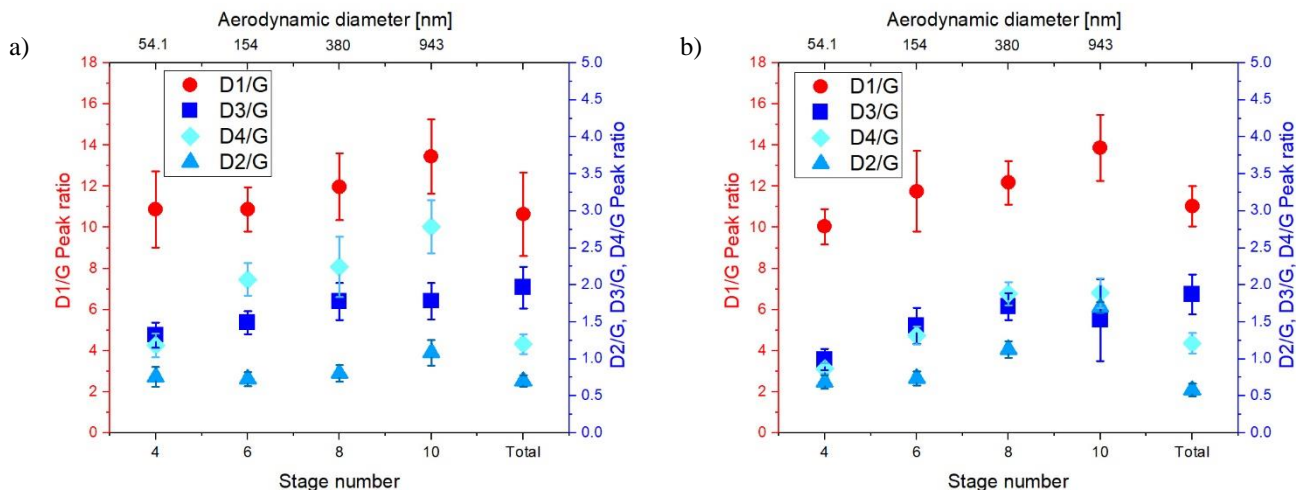
Figure S.6 Raman spectra of soot nanoparticles generated by an inverted burner fed with 0.13 lpm a) and 0.09 lpm b) of ethylene gas using the system shown in Figure S.4, including the use of building air without thermodenuder. Soot nanoparticles are collected on stages 4, 6, 8, and 10 of an ELPI+ impactor.

c) Building air with thermodenuder

In order to avoid the possibility of presence of any hydrocarbon in the building air, a thermodenuder was added to the experimental system shown in Figure S.4, as shown in Figure S.7.
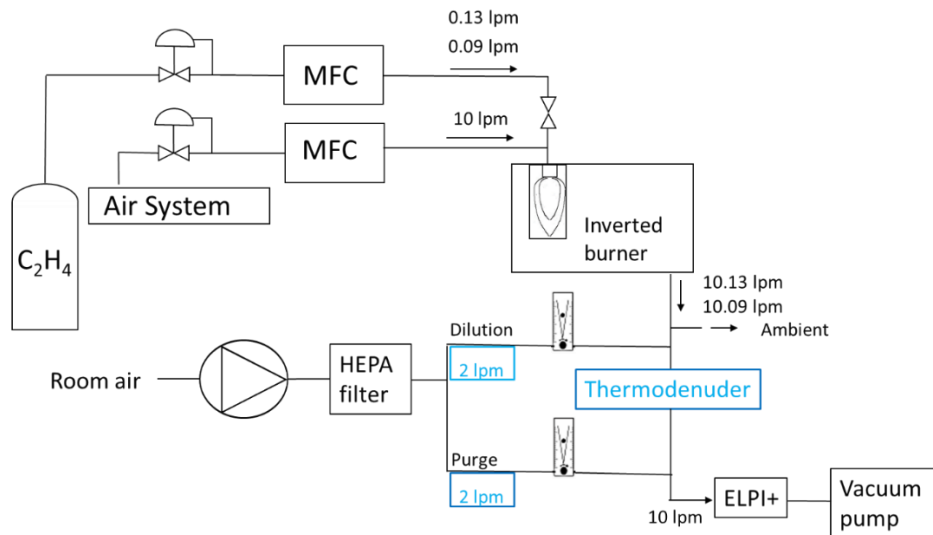
Figure S.7 Schematic of the experimental setup involving the use of the building air as source of the inverted burner combustion flame. A thermodenuder is used to reduce the hydrocarbons present in the building air.

Figure S.8 shows the distribution of number per each stage of ELPI+ for the test system shown in Figure S.7, building air with the use of thermodenuder. The trends of aggregates number recorded for the system of building air and thermodenuder (Figure S.8) and bottle air (shown in Figure 4 in the main publication) are very similar indicating that the results obtained by these two systems are comparable.
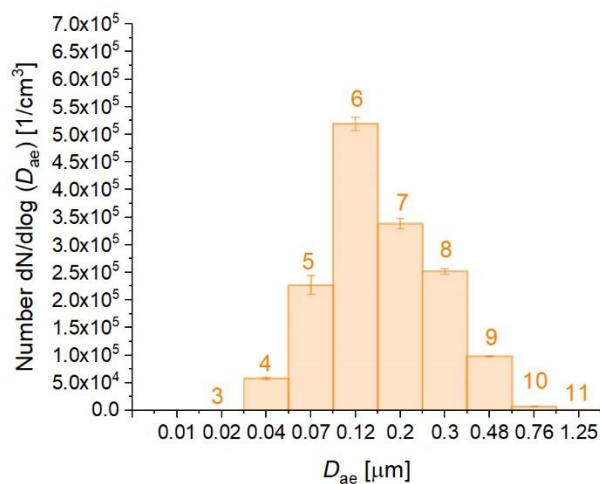
Figure S.8 Number distribution for each stage of the ELPI+ impactor for the setup shown in Figure S.7.

5

Figure S.9 shows the Raman spectra of soot generated by an inverted burner fed with 0.13 lpm and 0.09 lpm of ethylene gas and for the system shown in Figure S.7. All the peak ratios, D1/G, D2/G, D3/G, and D4/G decrease with stage number,

7

indicating that the disordered carbon content is higher for smaller projected area equivalent diameter. The results shown in Figure S.9 are the same to the results shown in the main publication (Figure 7); this strengthens the conclusions in the main publication.
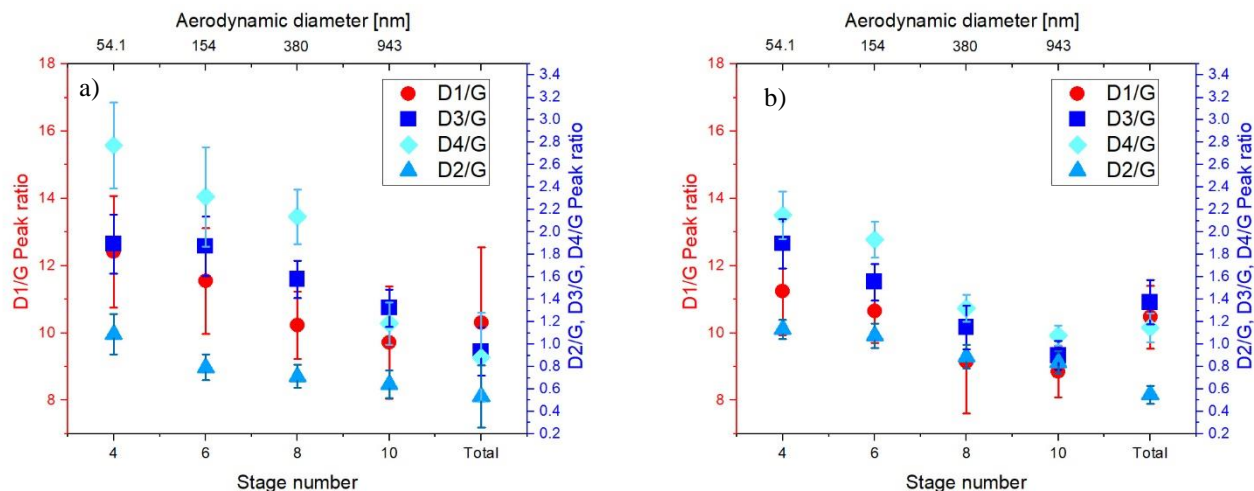
Figure S.9 Raman spectra of soot nanoparticles generated by an inverted burner fed with 0.13 lpm a) and 0.09 lpm b) of ethylene gas using the system shown in Figure S.7, including the use of building air and thermodenuder. Soot nanoparticles are collected on stages 4, 6, 8, and 10 of an ELPI+ impactor.

5 Summary of the results

Table S.2, S.3, S.4, S.5, S.6, and S.7 show the summary of peak ratios of the Raman spectra, showing their average and standard deviation values, for the Raman spectra obtained from different operating conditions and deconvolutions procedures.

.

Table S.2 Raman peak ratios obtained by the operating conditions of a) Bottled air, ethylene flow rate of 0.13 lpm and air flow rate of 10 lpm.

Stages	D1/G	D3/G	D2/G	D4/G
4	13.6 ± 2.4	2.16 ± 0.4	1.15 ± 0.2	2.17 ± 0.4
5	12.5 ± 0.9	2.10 ±0.2	1.19 ± 0.2	2.23 ± 0.19
6	11.7 ±2.3	2.05 ± 0.2	1.07 ± 0.2	1.88 ± 0.3
7	10.9 ± 1.6	1.89 ± 0.4	0.89 ± 0.2	1.71 ± 0.3
8	11.1 ± 0.6	1.87 ± 0.1	0.76 ± 0.1	1.01 ± 0.1
9	10.8 ± 2.0	1.15 ± 0.1	0.54 ± 0.1	0.71 ± 0.1
10	9.21 ± 1.9	0.92 ± 0.1	0.44 ± 0.1	0.64 ± 0.2
11	8.60 ± 2.0	0.71 ± 0.4	0.42 ± 0.2	0.54 ± 0.4
Total	11.1 ± 1.3	1.52 ± 0.1	0.98 ± 0.1	1.123 ± 0.1

Table S.3 Same data as above, but spectra background subtraction using linear baseline rather than titanium background.

Stages	D1/G	D3/G	D2/G	D4/G
4	10.6 ± 1.8	1.68 ± 0.3	0.90 ± 0.2	1.70 ± 0.2
5	10.6 ± 0.8	1.78 ± 0.2	1.01 ± 0.2	1.89 ± 0.1
6	10.4 ± 2.1	1.83 ± 0.2	1.01 ± 0.2	1.67 ± 0.3
7	10.4 ± 1.6	1.79 ± 0.4	0.84 ± 0.2	1.62 ± 0.2
8	11.3 ± 0.6	1.92 ± 0.1	0.82 ± 0.1	1.03 ± 0.1
9	10.3 ± 1.9	1.09 ± 0.1	0.51 ± 0.1	0.67 ± 0.1
10	10.2 ± 2.1	1.02 ± 0.2	0.49 ± 0.1	0.70 ± 0.2
11	8.01 ± 1.8	0.66 ± 0.4	0.39 ± 0.2	0.50 ± 0.3
Total	8.77 ± 1.0	1.21 ± 0.1	0.77 ± 0.1	0.89 ± 0.1

5

Table S.4 Raman peak ratios obtained by the operating conditions of building compressed air *without* thermodenuder, ethylene flow rate of 0.13 lpm and air flow rate of 10 lpm.

Stages	D1/G	D3/G	D2/G	D4/G
4	10.8 ± 1.8	1.32 ± 0.2	0.66 ± 0.1	1.19 ± 0.2
6	10.9 ± 1.1	1.49 ± 0.2	0.73 ± 0.1	2.07 ± 0.2
8	11.9 ± 1.6	1.78 ± 0.2	0.80 ± 0.1	2.25 ± 0.4
10	13.4 ± 1.8	1.79 ± 0.2	1.08 ± 0.2	2.79 ± 0.3
Total	10.6 ± 2.0	1.67 ± 0.3	0.71 ± 0.1	1.22 ± 0.1

Table S.5 As above, but for ethylene flow rate of 0.09 lpm.

Stages	D1/G	D3/G	D2/G	D4/G
4	10.1 ± 0.8	1.04 ± 0.1	0.69 ± 0.1	0.87 ± 0.1
6	11.7 ± 1.9	1.45 ± 0.2	0.74 ± 0.1	1.32 ± 0.1
8	12.6 ± 1.2	1.71 ± 0.2	1.13 ± 0.1	1.88 ± 0.1
10	13.8 ± 1.6	1.53 ± 0.6	1.27 ±0.1	1.89 ± 0.2
Total	11.1 ± 0.9	1.30 ± 0.5	0.73 ± 0.1	1.21 ± 0.1

Table S.6 Same as S.4 except that aerosol was stripped with a thermodenuder.

Stages	D1/G	D3/G	D2/G	D4/G
4	12.4 ± 1.6	1.89 ± 0.3	1.09 ± 0.2	2.77 ± 0.4
6	11.5 ± 1.6	1.87 ± 0.3	0.79 ± 0.1	2.31 ± 0.4
8	10.2 ±1.0	1.58 ± 0.2	0.71 ± 0.1	2.14 ± 0.2
10	9.71 ± 1.6	1.32 ± 0.2	0.64 ± 0.1	1.19 ± 0.2
Total	10.3 ± 2.2	0.93 ± 0.2	0.53 ± 0.3	0.88 ± 0.4

Table S.7 Same as S.5 except that aerosol was stripped with a thermodenuder.

Stages	D1/G	D3/G	D2/G	D4/G
4	11.2 ± 1.3	1.89 ± 0.2	1.13 ± 0.1	2.15 ± 0.2
6	10.6 ± 0.9	1.55 ± 0.2	1.08 ± 0.1	1.93 ± 0.2
8	9.14 ± 1.5	1.15 ± 0.2	0.89 ± 0.1	1.32 ± 0.1
10	8.85 ± 0.8	0.90 ± 0.1	0.84 ± 0.1	1.08 ± 0.1
Total	10.5 ± 0.9	1.37 ± 0.2	0.55 ± 0.1	1.15 ± 0.1

To test the stability of the deconvolution procedure, the total exhaust samples (as collected by TPS) of each operating condition were collected at a different times respect to the results shown in Table S.2, S.3, S.4, S.5, S.6 and S.7. The total exhausts obtained with different operating conditions have been collected using a thermophoretic particle sampler (TPS). The Raman spectra of the total exhausts were obtained and the disordered/ordered ratios are shown in Table S.8. The D1/G ratio differs at

5   most of 8.6 % indicating a high stability of the Raman deconvolution procedure.

Table S.8 Raman peak ratios of total exhausts obtained by different operating conditions. These peak ratios are obtained from soot exhausts collected at a different time respect to the results shown in Table S.2, S.4, S.5, S.6, and S.7.

Operating condition	Measurement time	D1/G	D3/G	D2/G	D4/G
a) Bottled air (0.13 lpm fuel)	Original	11.1 ± 1.3	1.52 ± 0.1	0.98 ± 0.1	1.123 ± 0.1
	Repeat	11.3 ± 1.0	1.32 ± 0.1	0.67 ± 0.1	1.38 ± 0.1
b) Building system (0.13 lpm fuel)	Original	10.6 ± 2.0	1.67 ± 0.3	0.71 ± 0.1	1.22 ± 0.1
	Repeat	11.2 ± 1.2	1.23 ± 0.1	0.64 ± 0.1	1.38 ± 0.1
b) Building system (0.09 lpm fuel)	Original	11.1 ± 0.9	1.30 ± 0.5	0.73 ± 0.1	1.21 ± 0.1
	Repeat	11.0 ± 1.0	1.30 ±0.1	0.56 ± 0.2	1.45 ± 0.2
c) Building system and thermodenuder (0.13 lpm fuel)	Original	10.3 ± 2.2	0.93 ± 0.2	0.53 ± 0.3	0.88 ± 0.4
	Repeat	11.2 ± 0.9	1.23 ± 0.1	0.63 ± 0.1	1.32 ± 0.1
c) Building system and thermodenuder (0.09 lpm fuel)	Original	10.5 ± 0.9	1.37 ± 0.2	0.55 ± 0.1	1.15 ± 0.1
	Repeat	10.4 ± 0.8	1.16 ± 0.1	0.70 ± 0.1	1.49 ± 0.2

References

Cloutis, E., Szymanski, P., Applin, D., and Goltz, D.: Identification and discrimination of polycyclic aromatic hydrocarbons using Raman spectroscopy, Icarus, 274, 211-230, 2016.

5 Cordeiro, D. S. and Corio, P.: Electrochemical and photocatalytic reactions of polycyclic aromatic hydrocarbons investigated by raman spectroscopy, Journal of the Brazilian Chemical Society, 20, 80-87, 2009.

Kazemimanesh, M., Moallemi, A., Thomson, K., Smallwood, G., Lobo, P., and Olfert, J. S.: A novel miniature inverted-flame burner for the generation of soot nanoparticles, Aerosol Science and Technology, 2018. 1-12, 2018.

Lappi, M. K. and Ristimäki, J. M.: Evaluation of thermal optical analysis method of elemental carbon for marine fuel exhaust, Journal of the Air & Waste Management Association, 67, 1298-1318, 2017.

10 Nowakowski, M., Rostkowski, P., and Andrzejewski, P.: Oxidized forms of polycyclic aromatic hydrocarbons (Oxy-PAHs): determination in suspended particulate matter (SPM), 15th International Conference on Environmental Science and Technology, 2017.